Life Sciences 217 (2019) 222–228

Contents lists available at ScienceDirect

Life Sciences

journal homepage: www.elsevier.com/locate/lifescie

Triazoles bind the C-terminal domain of SMO: Illustration by docking and molecular dynamics simulations the binding between SMO and triazoles

Musang Liu[a], Guanzhao Liang[a], Hailin Zheng[a], Nan Zheng[b], Hu Ge[c], Weida Liu[a,*]

[a] Department of Medical Mycology, Institute of Dermatology, Chinese Academy of Medical Science and Peking Union Medical College, Jiangsu Key Laboratory of Molecular Biology for Skin Diseases and STIs, Nanjing, Jiangsu, China
[b] Medical School, Nanjing University, Nanjing, Jiangsu, China
[c] Medical College, Qingdao University, Qingdao, China

ARTICLE INFO

Keywords:
Hedgehog signaling pathway
Smoothened
Triazoles
Itraconazole
Posaconazole

ABSTRACT

Itraconazole is an antagonist of the component Smoothened of Hedgehog pathway, which can inhibit the growth of medulloblastoma, basal cell carcinoma, and melanoma, etc. To research the binding mechanism of the Smoothened and triazoles, we used docking and molecular dynamics simulations on the Smoothened crystal structure and six triazoles. Unlike vismodegib, itraconazole can effectively bind into the pocket in the C-terminal domain of the Smoothened crystal structure instead of the N-terminal domain. The binding of itraconazole can change the conformation of the N-terminal domain even although itraconazole only had limited area contacting with N-terminal domain of the Smoothened. Besides, the binding of Itraconazole will not affect the binding of vismodegib. The strong binding affinity could be demonstrated between itraconazole and the Smoothened. Posaconazole and ketoconazole also had the strong binding affinity and the similar binding mode with the Smoothened crystal structure.

1. Introduction

As an efficient and safe triazole antifungal agent [1], itraconazole (ITZ) is also an potent antagonist of the Hedgehog (Hh) signaling pathway that inhibits cancer growth [2]. Through acting on the component Smoothened (SMO) of Hh pathway, ITZ can suppress the growth of medulloblastoma [2], basal cell carcinoma (BCC) [3], and malignant melanoma [4], etc. Posaconazole (PCZ), a second-generation triazole antifungal drug, can also suppress the growth of basal cell carcinoma by inhibiting Hh pathway, as with itraconazole [5].

The crystal structure of the multi-domain human SMO was reported and a precise arrangement of three distinct domains was revealed [6]. However, it still remains unclear how the ITZ molecule binds to SMO and inhibits the activity of SMO. To further study the interaction between SMO and triazoles, we used docking and molecular dynamics simulations to research on the binding of SMO crystal structure and 6 azoles, separately. We found that ITZ, PCZ, and ketoconazole (KCZ) had the similar binding mode with SMO, indicating valuable structure–-function relationships in biology. The simulations model gave insight into the feature requirements of the common backbone for the SMO inhibitory activity. Further, focusing on the SMO crystal structure and drug binding affinity may bring us more inspiration to design and synergize new drugs.

2. Methods

2.1. Docking and molecular dynamics (MD) simulations

Glide docking [2], part of the Schrödinger suite [8,9], and the docking algorithm in Molecular Operating Environment (MOE) [4] were carried out to prepare the protein-ligand complex. Here, the C-terminal domain (CTD) of the SMO crystal structure (PDB ID: 5L7D) [3] is treated as the targeted protein and the site around the ligand in the crystal structure is the binding pocket. Although ITZ is supposed to bind in the pocket of the C-terminal domain, N-terminal domain (NTD) is also regarded as part of the receptor in order to determine the function of this domain. The whole protein was protonated at pH of 7. The Glide XP scoring function [8,11] and the scoring function in MOE were employed to assess the binding mode and the best one was used as the initial structure in the MM MD simulations. Consequently, multi-step MM MD simulations were adopted in order to equilibrate the complex structure. Here the ff14SB force field [13] was used to describe the

* Corresponding author at: Institute of Dermatology, Chinese Academy of Medical Science and Peking Union Medical College, 12 Jiangwangmiao Street, Nanjing 210042, Jiangsu, China.
E-mail address: liumyco@hotmail.com (W. Liu).

https://doi.org/10.1016/j.lfs.2018.12.012
Received 22 October 2018; Received in revised form 3 December 2018; Accepted 8 December 2018
Available online 10 December 2018

protein and the gaff force field [5] to the ligand. The partial atomic charge of substrates was calculated by the restrained electrostatic potential (RESP) [6] charge from HF/6-31G* calculation with Gaussian 09 package [7]. In the ligand-receptor complex preparation, the system was neutralized by adding the counter ion (Na^+/Cl^-), and then solvated by a TIP3P cubic water box. The total volume was about $70 * 85 * 150\ Å^3$. In the MD simulations, first of all, three steps of minimization were carried out to optimize the water molecules, the side chains, and the whole system respectively. Then, 100 ps MD simulations under canonical ensemble with the Berendsen thermostat method [8] was used to heat up the system from 0 K to 300 K, and another 100 ps MD simulations under isobaric ensemble to equilibrate the system. Finally, 50 ns MD simulations under NVT were applied to relax the binding of the protein-ligand complex. The Particle mesh Ewald (PME) method was employed to treat long-range electrostatic interactions. The cutoff values for both van der Waals interactions and electrostatic interactions were 10 Å. Shake algorithm [9] was used to constrain all hydrogen-containing bonds with a tolerance of 10^{-5}. The time step was chosen as 2 fs. All the MM MD simulations were performed with pmemd.cuda [10] in AMBER14 [15]. After a long time MD simulations, MM-PBSA was used to calculate the binding free energy between the ligand and the protein. Moreover, dihedral principal component analysis (dPCA) [11] was applied to analyze the conformational change of the protein.

3. Results

3.1. Docking

Five classical triazole antifungal agents, namely ITZ, fluconazole (FNZ), miconazole (MNZ), KCZ and clotrimazole (CTZ) (in Scheme 1), were prepared for the comparison of the different performances between the triazole and SMO. Here the docking results of these five ligands and the cholesterol (the original ligand in the crystal structure) based on the Glide XP and MOE scoring function have been listed in Table 1. Apparently, the binding affinity between SMO and ITZ is higher than those between SMO and fluconazole, miconazole and clotrimazole, which is corresponding to the previous experiments. Additional, the docking results indicate that the binding affinity between SMO and KCZ is close to the value of ITZ and both of these two ligands have the similar affinities with SMO to the cholesterol, which is the endogenous ligand of SMO.

Table 1
The docking results of SMO and five classical triazole antifungal agents.

Scoring function	MOE	Glide XP
ITZ	2	1
CTZ	5	5
KCZ	1	2
MNZ	3	3
FNZ	4	4

3.2. MD simulations and binding free energies

By employing the structures after docking, the extensive MD simulations (100 ns for each ligand-protein complex) have been carried out to determine the exact binding mode and binding free energies between SMO and the triazoles in order to figure out the causes for the higher binding affinity between SMO and ITZ than those between SMO and most of the other triazoles. As illustrated in Fig. 1(a), hydrophobic interactions are dominant in the binding between SMO and ITZ. Owing to the existence of several aromatic rings in ITZ, many residues in both CTD and NTD form the CH-π interactions with ITZ, including Leu55, Val523, Leu524, Cys525 and the other non-polar residues. Besides, a cation-π interaction between Arg104 and one of the aromatic rings in ITZ increases the binding affinity between SMO and ITZ. Although no direct hydrogen bond exists, there is an indirect hydrogen bond between Tyr150 and the carboxyl group of ITZ.

In order to determine the binding affinity between SMO and ITZ, the binding between SMO and its endogenous ligand, cholesterol, has been set as the reference. With the same MD procedures, the binding mode of SMO and cholesterol has been shown in Fig. 1(b). Apparently, the binding mode between SMO and cholesterol is disparate from that of

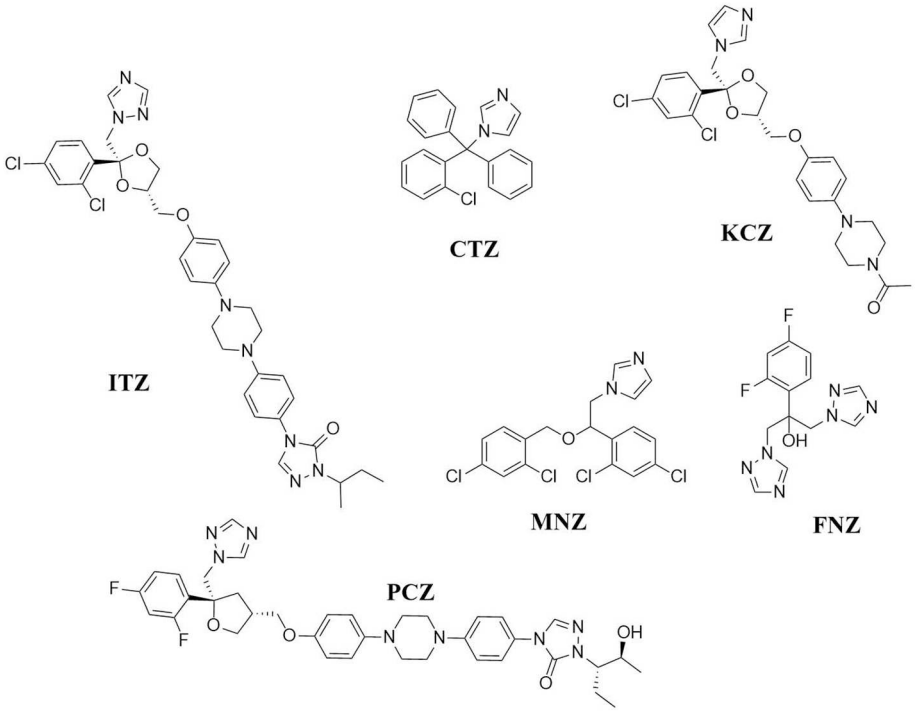

Scheme 1. The structures of six classical triazole antifungal agents.

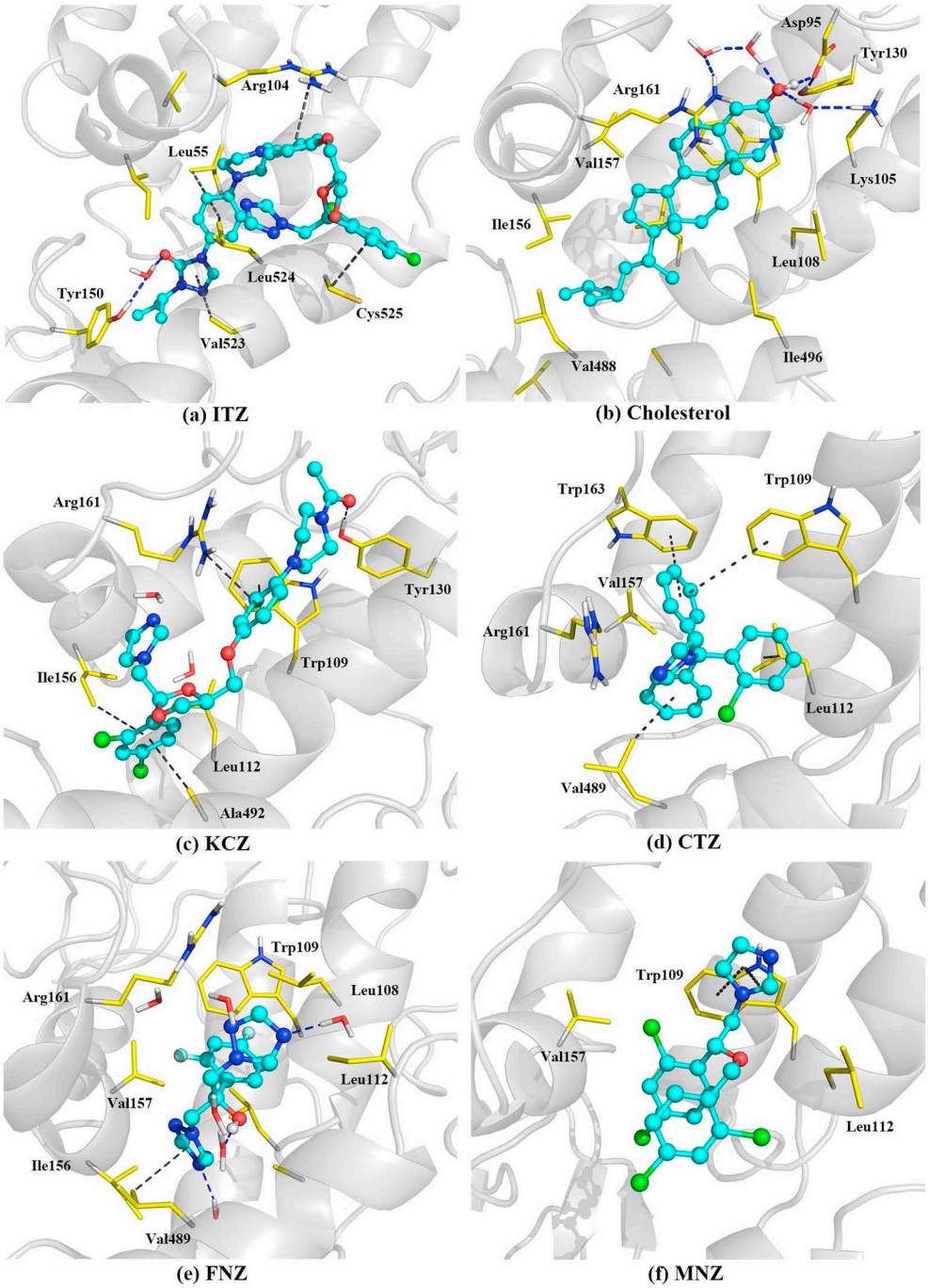

Fig. 1. The binding mode of ITZ, cholesterol, KCZ, CTZ, FNZ, MNZ and SMO. Herein, the hydrogen bonds are shown in blue dash lines while the hydrophobic interactions are shown in black. (a) Obviously, the hydrophobic interactions, especially the CH-π interactions, are dominant in the ligand-protein binding interaction. Besides, the indirect hydrogen bond and the cation-π interaction between ITZ and Tyr150, and Arg104 respectively contribute to the affinity of the ligand and the protein. (b) Although there is no aromatic ring in cholesterol, it still has a strong hydrophobic interaction with many non-polar residues in CTD and even in NTD (Val 488, Ile496 and Ala492). (c)–(f) The hydrophobic interaction is still dominant for these four triazoles binding with SMO. (For interpretation of the references to colour in this figure legend, the reader is referred to the web version of this article.)

SMO and ITZ. Strong hydrogen bond interactions are dominant in the binding between SMO and cholesterol. However, owing to the lack of aromatic ring in cholesterol, few CH-π interactions exist. Furthermore, due to the amphipathic property of cholesterol, hydrophobic interactions between the hydrophobic part of cholesterol and the non-polar residues from CTD and NTD play a role in the binding.

Since it is unable to determine the binding affinity through the comparison of the binding mode between SMO and ITZ and the one between SMO and cholesterol, MM-PBSA, which is a general method for the binding free energy calculations, is employed to quantify the binding affinity of SMO and ITZ. As listed in Table 2, the binding free energies of the structures in the last two nanoseconds have been calculated. According to the results of MM-PBSA, the binding free energy of SMO and ITZ is the one which is closest to that of SMO and cholesterol, while those triazoles have the much less negative binding free energies with SMO than the one of SMO and ITZ. Both of these results indicate that ITZ can bind with CTD of SMO effectively which is consistent to the experimental result.

Besides the binding mode between SMO and ITZ or cholesterol, the possible binding modes between SMO and other four triazoles (KCZ, CTZ, FNZ, and MNZ) have been discussed in the following part. Finally, another triazole, PCZ, which has been proved as the inhibitor for the SMO [5], was chosen to validate the model. As shown in Fig. 1, the hydrophobic interaction is still dominant in the binding modes of these four kinds of triazoles. However, the polar interactions in these four binding modes, such as cation-π and hydrogen bond, contribute less than one in the binding modes between SMO and ITZ or cholesterol. In addition, fewer residues in NTD interact with these four triazoles than that with ITZ or cholesterol. All of these result in the decrease of the binding affinity of these four triazoles with SMO.

Table 2
The binding free energy (BFE) between SMO and five triazoles and cholesterol.

BFE	Cholesterol	ITZ	KCZ	FNZ	MNZ	CTZ
MMPBSA	**−39.53 ± 2.30**	**−39.08 ± 5.06**	−32.55 ± 4.66	−14.97 ± 2.54	−22.27 ± 2.53	−12.78 ± 3.34

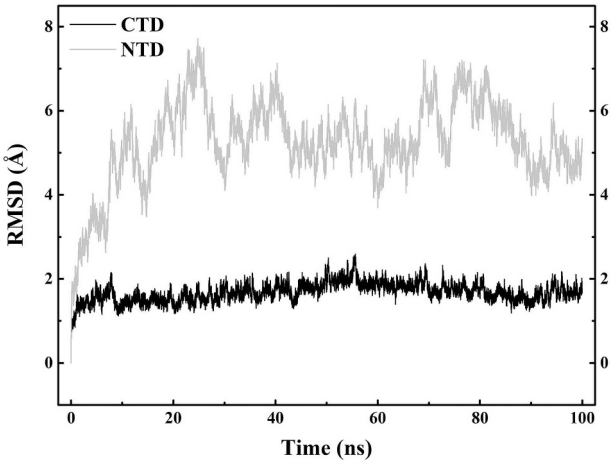

Fig. 2. The RMSDs along the MD simulations of C-terminal domain (CTD) and N-terminal domain (NTD). Based on the RMSD values, the CTD is very stable during the simulations whereas the NTD is fluctuating.

3.3. Conformational change and dPCA results

According to the root-mean-square deviation (RMSD) in Fig. 2, the fluctuations of the CTD and NTD are totally different. Although the binding pocket is located in the CTD, the fluctuation of the NTD is larger than that of the CTD. The RMSD of the CTD fluctuates around 1.75 Å after 5 ns while the RMSD of the NTD fluctuates around 5 Å (in Fig. 2). In order to determine the change of the NTD, the dPCA has been carried out to analyze the conformational change of the NTD. Herein, the results of dPCA have been depicted in Fig. 3(a,b). The change of conformation of the NTD is larger than that of CTD even though the conformation of the CTD also changes. According to the conformation evolution in Fig. 4(a), the conformational change of the CTD is mostly contributed by one of the loops, which is far way from the binding pocket, while the conformational change of the NTD contains the change of the part close to the binding pocket. These indicate that the binding of ITZ in the CTD can induce the conformational change of the NTD. Furthermore, the dPCA method was also employed to calculate the conformational change of SMO binding with cholesterol. Similar conformational change of the NTD has been observed in the MD simulations. The dPCA results of SMO and cholesterol share many similarities with the those of SMO and ITZ, no matter the range or the shape of the change pathway. This similar conformational change provides another evidence to show that the binding affinity of ITZ with SMO is similar to the endogenous ligand, cholesterol.

Furthermore, the dPCA method has been carried out to analyze the conformational change of the NTD of the SMO-KCZ, SMO-CTZ, SMO-FNZ and SMO-MNZ as well (Fig. 3). Comparing these four dPCA results and the results from SMO-ITZ or SMO-cholesterol, the ranges in the SMO-ITZ and SMO-cholesterol (larger than 8) are apparently larger than the ranges of the other four systems (about 6). In these four dPCA results, only the range of the SMO-KCZ complex is close to the SMO-ITZ complex. Also, the binding energy of the SMO-KCZ complex is only 7 kcal/mol less than that of the SMO-ITZ complex, which means this triazole could be able to bind with SMO to some extent. Plus, the conformational change after binding into SMO makes the KCZ possible to control the signal of SMO similar to the ITZ. As for the other triazoles (CTZ, FNZ, and MNZ), due to their small scaffold and binding modes (Fig. 1), they are all unable to have a strong interaction with the NTD in SMO leading to the less conformational change in these three systems than the others.

3.4. Noncompetitive inhibition between vismodegib and triazoles

According to the previous experimental results, ITZ inhibits the SMO is noncompetitive with the triazoles. Two parallel simulations have been setup to demonstrate the noncompetitive inhibition mechanism between ITZ, vismodegib (VIG) and SMO. Based on the binding mode and binding energy analysis in Fig. 4(b) and Table 3, the binding modes between VIG and SMO with and without ITZ are similar. Both of these two systems have the T-stacking binding between the Trp225 and the aromatic ring of VIG. Besides, the phenol group in Tyr329 has a strong hydrogen bonding with the N in VIG. In addition, the hydrogen bond between the Asp319 and the carbonxyl group in VIG contributes to the binding between ligand and protein. In the VIG with ITZ model, an extra hydrogen bond between NH and Arg335 while in the VIG without ITZ model, the hydrogen bond has been found between P-O and Asn163. Several nonpolar interaction (T-stacking between Phe326 and ligand in the model with ITZ, T-stacking between Phe166 and ligand, and π-π stacking between Asn534 and ligand in the model without ITZ) between ligand and protein have been found as well. Although the binding modes between VIG and SMO are not exactly the same, their binding free energies are similar to each other. As the data shown in Table 3, the binding free energy of VIG and SMO is not affected by the existence of the ITZ while the existence of VIG does not influence the binding of ITZ and SMO. Therefore, the inhibition between VIG, ITZ and SMO is noncompetitive.

3.5. Validation

In order to validate the model that predicts the possible triazole inhibitors for the SMO, here another triazole compound, posaconazole (PCZ), was chosen. The same docking and MD procedures were employed for the PCZ-SMO complex and the binding result is depicted in Fig. 4. According to the binding mode, the binding interaction between PCZ and SMO is formed by two hydrogen bonds and several π-π/CH-π stackings. Residue Tyr73 forms a hydrogen bond with the O atom in the ligand via a water molecule, and Arg 104 forms a hydrogen bond directly with the N in the 1,2,4-triazole in the ligand. The binding free energy between the SMO and the PCZ is about 37 kcal/mol, which is 3 kcal/mol higher than the binding free energy between the SMO and the ITZ and much lower than the other SMO-ligand complexes (CTZ, FNZ, and MNZ). Therefore, our model that combined the MD simulations and binding free energy calculations can accurately predict the binding affinity between SMO and triazoles.

4. Discussion

The SMO is a key component of Hh signaling pathway, which regulates embryonic development and adult stem cells in animals [16,17]. The crystal structure of SMO was reported and well studied [6,18]. It was found the human SMO had three distinct domains: a seven-transmembrane helices domain, a hinge domain and an intact extracellular cysteine-rich domain [6]. Uncontrolled activation of the Hh pathway can lead to cancers in the brain, muscle, and skin, etc. [12]. ITZ, KCZ, and PCZ can inhibit the Hh signaling pathway and the progress of BCC, prostate cancer, colorectal cancer, melanoma, etc. [2,4,5] [13].

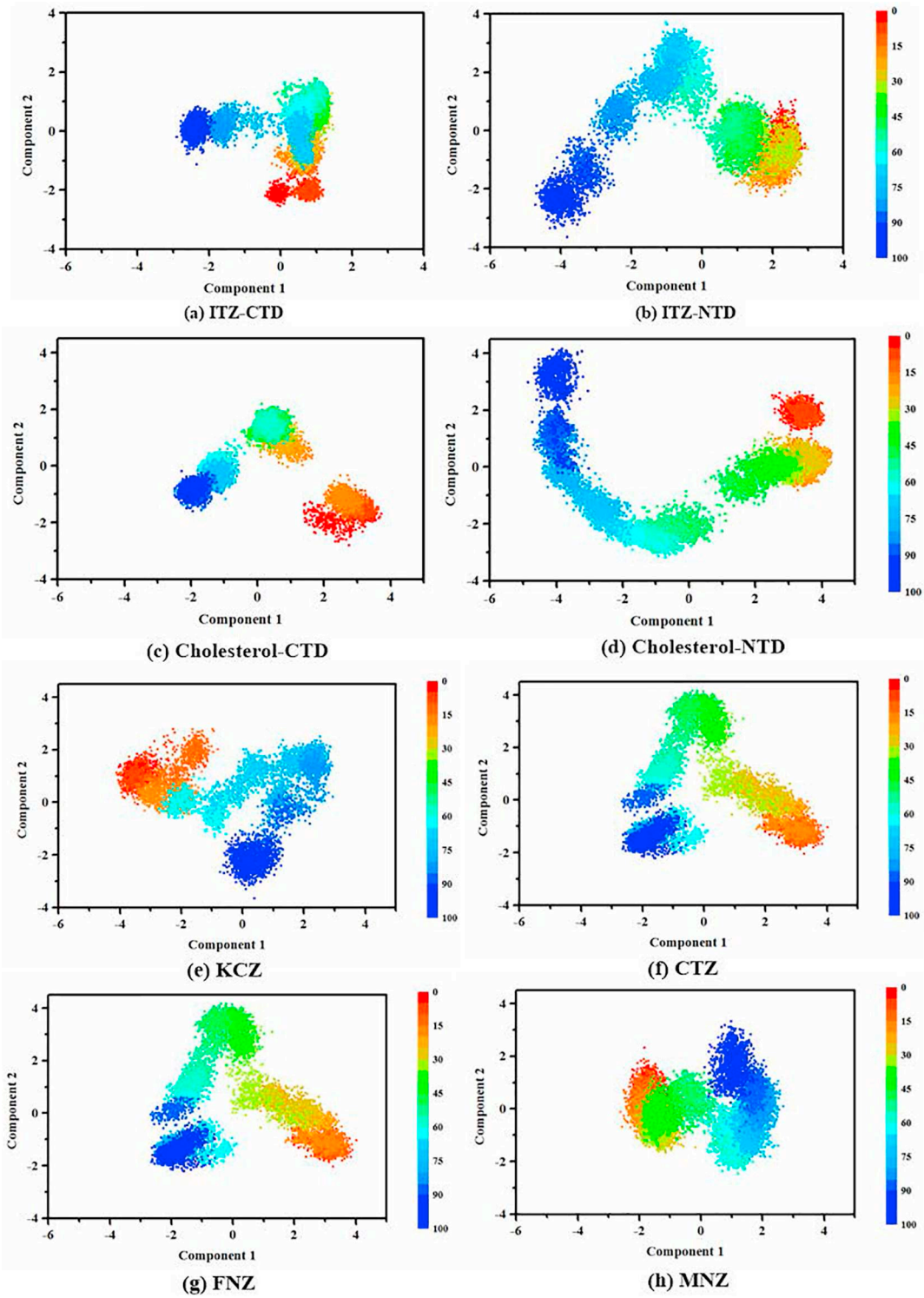

Fig. 3. The dPCA results of the CTD and NTD of SMO based on 100 ns MD simulations of SMO-ITZ complex (a,b), SMO-cholesterol complex (c,d). The dPCA results of the NTD of SMO based on 100 ns MD simulations of SMO-KCZ complex (e), SMO-CTZ complex (f), SMO-FNZ complex (g) and SMO-MNZ complex (h).

In our results, unlike other traditional ligands (such as the VIG), the ITZ can effectively bind into the pocket in the CTD of SMO. The binding of ITZ to SMO could cause the conformational change of the NTD even though it only has a small contact area with the NTD. Although the binding modes differ from each other (π-relative interactions are dominant in ITZ-SMO while a strong hydrogen bond interaction makes a large contribution to the cholesterol-SMO binding), the comparable binding free energies between ITZ-SMO complex and cholesterol-SMO complex (−39.1 kcal/mol vs. −39.5 kcal/mol) demonstrate the strong binding affinity between SMO and ITZ which is consistent to the experimental data. In addition, the binding of ITZ to the CTD of SMO would not affect the binding of the traditional SMO ligands (VIG), and vice versa. The VIG-SMO binding free energies change slightly (about 1 kcal/mol) between the model with ITZ and the model without ITZ. This is a strong evidence of the fact that ITZ and VIG are the non-competed ligands binding to SMO.

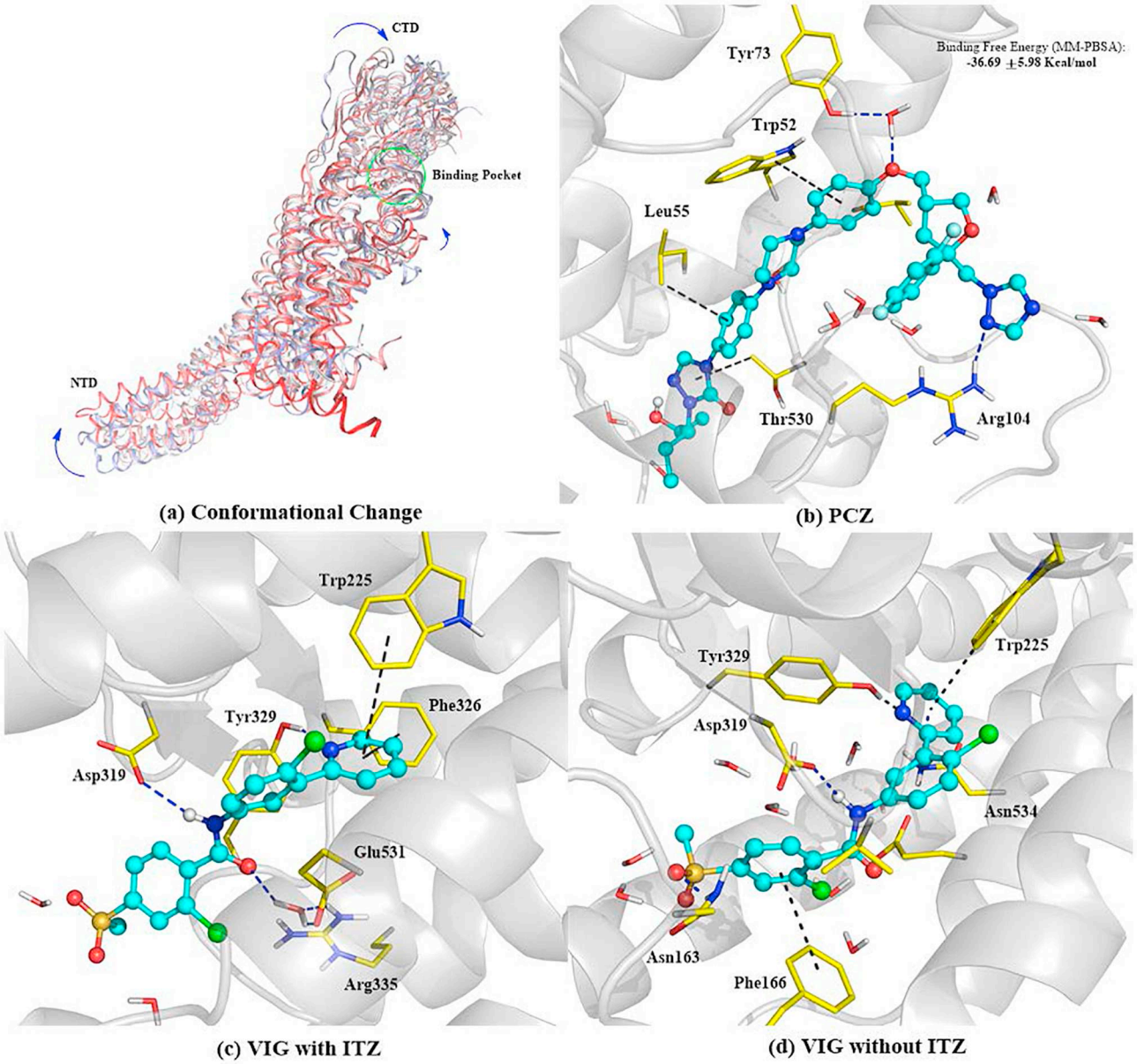

Fig. 4. (a) The conformation evolution during the MD simulations. The conformation changes have occurred for the loop* and the helix* in NTD. The loop* rotates clockwise a little bit and comes close to the pocket of CTD which results in interacting with the ligand, ITZ. As for the Helix*, it also rotates clockwise. Both these changes add up to the conformation change of NTD. (b) The possible binding mode of PCZ and SMO. Herein, the hydrogen bonds are shown in blue dash lines while the hydrophobic interactions are shown in black. The binding free energy is shown in the top right of the figure. (c) The comparison of the vismodegib (VIG) and SMO binding modes between the model with ITZ and the model without ITZ. The hydrogen bonds are shown in blue dash lines while the π stacking interactions are displayed in black dash lines. (For interpretation of the references to colour in this figure legend, the reader is referred to the web version of this article.)

Table 3
The binding free energy (BFE) between SMO and vismodegib in the model with ITZ and the model without ITZ.

BFE	VIG (w/ ITZ)	VIG (wo/ ITZ)	ITZ (w/ VIG)	ITZ (wo/ VIG)
MMPBSA	−26.69 ± 4.29	−25.65 ± 5.86	−40.96 ± 4.48	−39.08 ± 5.06

Besides, the PCZ, which is another known SMO triazole ligand, validates the correctness of our model. Not only the binding free energy, but also the binding mode of PCZ-SMO complex is similar to those of the ITZ-SMO complex (36.7 kcal/mol vs. 39.1 kcal/mol, and π-relative interactions are dominant in both complexes). Based on this model, another possible triazole ligand, KCZ, has a similar binding mode with SMO comparing to ITZ-SMO binding. Although the KCZ-SMO binding free energy is smaller than that of the ITZ-SMO complex (32.6 kcal/mol vs 39.1 kcal/mol), this binding free energy value is much larger than the values of the triazoles (CTZ, MNZ and FNZ) binding to SMO. At the same time, the KCZ binding to SMO would change the NTD conformation as well which is similar to the behavior of the ITZ-SMO complex. In comparison with ITZ [14] and PCZ [13], it was found that CTZ, MNZ and FNZ much more weakly inhibit Hh

pathway, in parallel with binding affinity of SMO crystal structure. However, it was examined that ketoconazole has weaker inhibitory effects on Hh pathway activity, with a 10-fold higher IC50 than that of itraconazole, indicating an inconsistent phenomenon between binding affinity and functional effects which need a further study.

In summary, we used docking and MD simulations to analysis how azoles binding the SMO crystal structure. The precise binding areas were calculated and the binding energy is compared. These results are useful to the anti-cancer study of azoles, which also can inspire the design and synergize of new drugs.

CRediT authorship contribution statement

Musang Liu: Conceptualization, Funding acquisition, Supervision, Writing - original draft. **Guanzhao Liang:** Data curation, Writing - review & editing. **Hailin Zheng:** Investigation, Visualization. **Nan Zheng:** Formal analysis, Validation. **Hu Ge:** Methodology, Software. **Weida Liu:** Project administration, Resources, Writing - review & editing.

Acknowledgments

The research was supported by the National Natural Science Foundation of China, China (Grant No. 81501726), the Natural Science Foundation of Jiangsu Province, China (Grant No. BK20150069), PUMC Youth Fund and the Fundamental Research Funds for the Central Universities, China (No. 3332016109), CAMS Innovation Fund for Medical Science, China (CAMS-I2M, 2016-I2M-3-021) and the National Natural Science Foundation of China (Grant No. 81603026).

References

[1] M. Haria, H.M. Bryson, K.L. Goa, Itraconazole. A reappraisal of its pharmacological properties and therapeutic use in the management of superficial fungal infections, Drugs 51 (4) (1996) 585–620.
[2] R. Friesner, et al., Flexible ligand docking with glide: evaluation of structure prediction performance and utility for virtual ligand screening, Abstr. Pap. Am. Chem. Soc. 223 (2002) U465.
[3] E.F. Byrne, et al., Structural basis of Smoothened regulation by its extracellular domains, Nature 535 (7613) (2016) 517–522.
[4] MOE, C.C.G. 2010.
[5] J.M. Wang, et al., Development and testing of a general amber force field, J. Comput. Chem. 25 (9) (2004) 1157–1174.
[6] C.I. Bayly, et al., A well-behaved electrostatic potential based method using charge restraints for deriving atomic charges - the Resp model, J. Phys. Chem. 97 (40) (1993) 10269–10280.
[7] M. Frisch, et al., Gaussian 09 Rev. D01, Gaussian, Inc., Wallingford, CT, 2012 (There is no corresponding record for this reference).
[8] H.J.C. Berendsen, et al., Molecular-dynamics with coupling to an external bath, J. Chem. Phys. 81 (8) (1984) 3684–3690.
[9] J.P. Ryckaert, G. C., H.J.C. Berendsen, Numerical integration of the cartesian equations of motion of a system with constraints: molecular dynamics of n-alkanes, J. Comput. Phys. 23 (1977) 327–341.
[10] R.E. Duke, L.G. Pedersen, PMEMD: a high performance implementation of AMBER molecular dynamics, Abstr. Pap. Am. Chem. Soc. 237 (2009).
[11] A. Altis, et al., Dihedral angle principal component analysis of molecular dynamics simulations, J. Chem. Phys. 126 (24) (2007).
[12] M. Pasca di Magliano, M. Hebrok, Hedgehog signalling in cancer formation and maintenance, Nat. Rev. Cancer 3 (12) (2003) 903–911.
[13] B. Chen, et al., Posaconazole, a second-generation triazole antifungal drug, inhibits the hedgehog signaling pathway and progression of basal cell carcinoma, Mol. Cancer Ther. 15 (5) (2016) 866–876.
[14] J. Kim, et al., Itraconazole, a commonly used antifungal that inhibits Hedgehog pathway activity and cancer growth, Cancer Cell 17 (4) (2010) 388–399.
[15] L. Zhao, et al., Corrigendum: Lanosterol reverses protein aggregation in cataracts, Nature 526 (7574) (2015) 595.
[16] P.W. Ingham, A.P. McMahon, Hedgehog signaling in animal development: paradigms and principles, Genes Dev. 15 (23) (2001) 3059–3087.
[17] D.J. Robbins, D.L. Fei, N.A. Riobo, The Hedgehog signal transduction network, Sci. Signal. 5 (246) (2012) re6.
[18] C. Wang, et al., Structure of the human smoothened receptor bound to an antitumour agent, Nature 497 (7449) (2013) 338–343.